Thermally Stable All-Polymer Solar Cells with High Tolerance on Blend Ratios

Yannan Zhang, Yalong Xu, Michael J. Ford, Fangchao Li, Jianxia Sun, Xufeng Ling, Yongjie Wang, Jinan Gu, Jianyu Yuan, and Wanli Ma**

Tuning the blend composition is an essential step to optimize the power conversion efficiency (PCE) of organic bulk heterojunction (BHJ) solar cells. PCEs from devices of unoptimized donor:acceptor (D:A) weight ratio are generally significantly lower than optimized devices. Here, two high-performance organic nonfullerene BHJ blends PBDB-T:ITIC and PBDB-T:N2200 are adopted to investigate the effect of blend ratio on device performance. It is found that the PCEs of polymer-polymer (PBDB-T:N2200) blend are more tolerant to composition changes, relative to polymer-molecule (PBDB-T:ITIC) devices. In both systems, short-circuit current density (J_{sc}) is tracked closely with PCE, indicating that exciton dissociation and transport strongly influence PCEs. With dilute acceptor concentrations, polymer-polymer blends maintain high electron mobility relative to the polymer-molecule blends, which explains the dramatic difference in PCEs between them as a function of D:A blend ratio. In addition, polymer-polymer solar cells, especially at high D:A blend ratio, are stable (less than 5% relative loss) over 70 d under continuous heating at 80 °C in a glovebox without encapsulation. This work demonstrates that all-polymer solar cells show advantage in operational lifetime under thermal stress and blend-ratio resilience, which indicates their high potential for designing of stable and scalable solar cells.

1. Introduction

High performance organic solar cells (OSCs) normally employ a sandwich-type configuration containing a donor:acceptor (D:A) bulk heterojunction (BHJ) blend.[1] Typical BHJ active layers are comprised of a conjugated polymer as the electron donor and a fullerene derivative as the electron acceptor.[2,3] Conventional fullerene acceptors like [6,6]-phenyl-C61 butyric acid methyl ester (PCBM) may be unfavorable for practical application, due to the inefficient absorption in visible and near-infrared (IR) regions, fixed molecular structure, complex purification process, and other complications well-documented in the literature.[4–8] In addition, the morphology of polymer-fullerene blends is very sensitive to thermal annealing, solvent additive, film thickness, and especially D:A ratio, resulting in significantly different device performance.[9–11] Recently, people have shown that the integration of either polymeric or molecular acceptor into photovoltaic devices would be advantageous. The chemical structures of nonfullerene acceptor can be easily adjusted to tune their energy levels, and the conjugated molecule or polymer acceptor demonstrates enhanced absorption at long wavelengths relative to fullerenes.[12] Thus nonfullerene photovoltaics can have improved harvest of solar radiation, enhanced thermal and mechanical stability, and reduced open-circuit voltage loss.[13] To date, solution-processed nonfullerene solar cells based on polymer–polymer (all-polymer) and polymer-small molecule blend have achieved power conversion efficiencies (PCEs) of 10% and 13%, respectively.[14–19]

Exciton dissociation and charge transport are at the core of organic photovoltaics, which is strongly affected by the BHJ blend morphology.[20–23] In fullerene-based systems, the morphology of thin films is critical to the device performance and has been extensively studied.[24] How the blend morphology of nonfullerene blend affects device efficiency and stability is of growing interest as the PCEs of many nonfullerene solar cells now exceed the best fullerene devices. It is well known that the morphology has been largely influenced by the D:A blend ratio. Early studies on fullerene-based devices observed a drastic change in film morphology when fabricating the devices with increased acceptor content.[25–28] However, for nonfullerene solar cells, recent efforts mainly focus on materials synthesis and device optimization. To the best of our knowledge, systematical study on the effect of blend ratio on the device morphology, performance, and stability has not been reported, while it is of great importance to help achieve in-depth

Y. Zhang, Y. Xu, F. Li, J. Sun, X. Ling, Y. Wang, J. Gu,
Prof. J. Yuan, Prof. W. Ma
Institute of Functional Nano and Soft Materials (FUNSOM)
Jiangsu Key Laboratory for Carbon-Based Functional Materials and Devices
Joint International Research Laboratory of Carbon-Based Functional Materials and Devices
Soochow University
199 Ren-Ai Road, Suzhou Industrial Park
Suzhou, Jiangsu 215123, P. R. China
E-mail: jyyuan@suda.edu.cn; wlma@suda.edu.cn

M. J. Ford
Center of Polymers and Organic Solids
Materials Department
University of California, Santa Barbara
Santa Barbara, CA 93106, USA

The ORCID identification number(s) for the author(s) of this article can be found under https://doi.org/10.1002/aenm.201800029.

DOI: 10.1002/aenm.201800029

understanding of this emerging new photovoltaic technology. Especially, we notice less attention has been paid to all-polymer solar cells since their efficiency is relatively lower than polymer–molecule system. Therefore, the potential merits of all-polymer solar cells have not been fully recognized.

The compounds 3,9-bis(2-methylene-(3-(1,1-dicyanomethylene)-indanone))-5,5,11,11-tetrakis(4-hexylphenyl)-dithieno[2,3-d:2′,3′-d′]-s-indaceno[1,2-b:5,6-b′]dithiophene (ITIC) and poly((N,N′-bis(2-octyldodecyl)-1,4,5,8-naphthalenedicarboximide-2,6-diyl)-alt-5,5′-(2,2′-bithiophene)) (N2200) (see **Figure 1**) are among the highest performing and most widely studied nonfullerene acceptors. poly[(2,6-(4,8-bis(5-(2-ethylhexyl)thiophen-2-yl)-benzo[1,2-b:4,5-b′]dithiophene))-alt-(5,5-(1′,3′-di-2-thienyl-5′,7′-bis(2-ethylhexyl)benzo[1′,2′-c:4′,5′-c′]dithiophene-4,8-dione))] (PBDB-T):ITIC and PBDB-T:N2200 are efficient polymer:molecule and all-polymer blends for nonfullerene solar cells, respectively.[29,30] With appropriate interlayers and processing additives, PCEs as high as 11.3% and 7% have been achieved, respectively.[31] The similar processing conditions of these two blend films make it feasible to comparatively study the effect of polymeric and molecular acceptor on device morphology and stability behaviors, while maintaining a high level of device performance. In this report, we compared the device performance of nonfullerene solar cells utilizing aforementioned polymeric and molecular acceptors with a wide range of blend ratios. We also investigated their device stability under continuous heating at 80 °C over 70 d. It is worth noting that residual additive 1,8-diiodooctane (DIO) within the film has been implicated as the cause of slow changes in morphology over time, which impact device performance and stability.[32–34] Thus we fabricated solar cell devices without using DIO to exclude the complication of additive. The resultant devices still exhibited comparable PCEs compared to the optimal devices using additive,[13] which makes it simpler to focus on the effect of blend ratio on the device stability under long-time thermal stress.

We comprehensively investigated the influence of D:A blend ratio on the performance of all-polymer solar cells (PBDB-T:N2200) and polymer–molecule solar cells (PBDB-T:ITIC). The champion solar cells based on ITIC and N2200 produce highest PCEs approaching 10% and over 6%, respectively. We then systematically adjusted the D:A ratios from 1:10 to 20:1 to investigate the vast change on the device morphology and performance. Based on the results, we defined three regions of the D:A ratio: Region I (high acceptor content): 1:10 to 1:3; Region II (optimal content): 1:3 to 3:1; Region III (low acceptor content): 3:1 to 20:1. With ultrahigh content of acceptor, both ITIC and N2200-based devices showed relatively low PCE values. Upon the loading of more donor polymer PBDB-T, the PCE quickly increased and the maximum value was achieved in Region II. Quite interestingly, in Region III, the decrease of PCE with largely reduced acceptor content was significantly different for devices based on ITIC and N2200. The PCE of PBDB-T:ITIC cell undergoes a drastic decrease to almost 0% at a D:A ratio around only 10:1, which is similar to the observation in polymer-fullerene solar cells.[26] In contrast, the PBDB-T:N2200 cell can still impressively maintain over 60% of the maximum PCE. Moreover, with an extremely low D/A ratio of 20:1, the PCE can still maintain over 40% of the original value. This interesting phenomenon has never been reported and may have significant impact on the future progress of nonfullerene solar cells. The working mechanisms and resultant device stability of the solar cells with ultralow acceptor content are not clear. We therefore investigated the charge carrier generation, transfer and transport

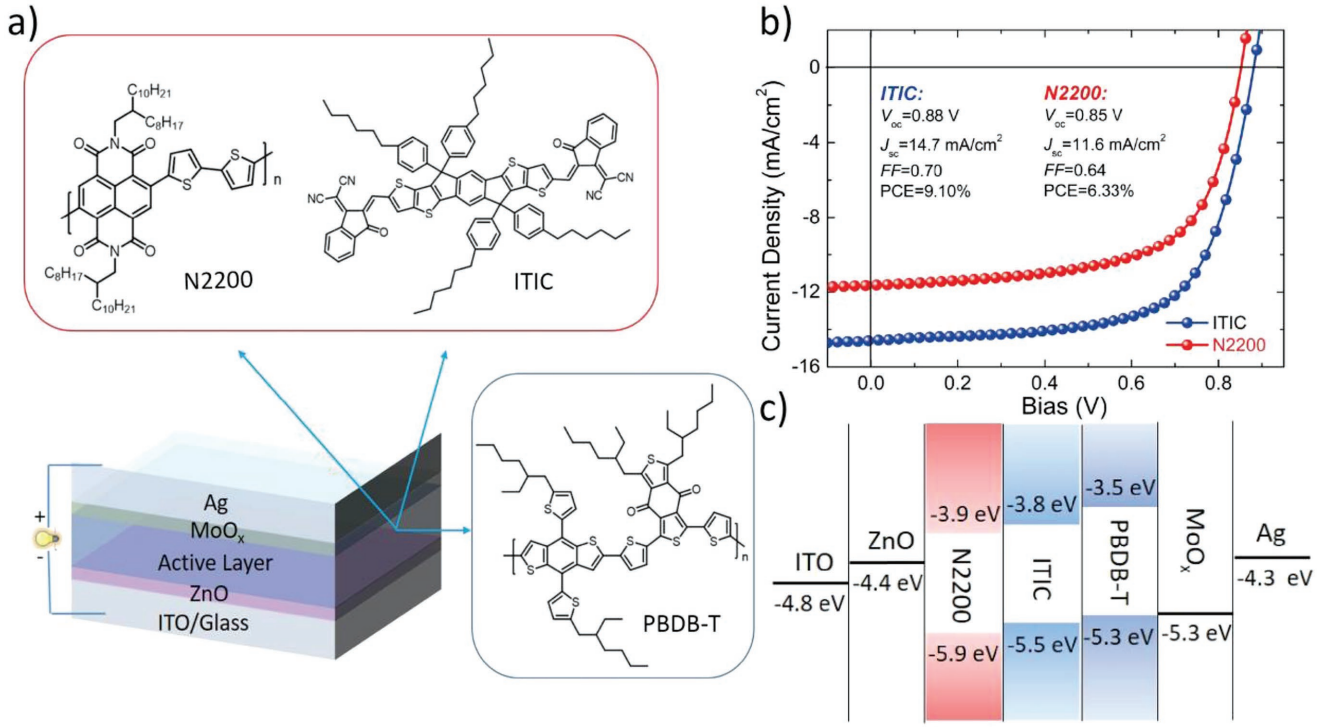

Figure 1. a) Chemical structures of PBDB-T, N2200, and ITIC, and device structure of inverted polymer solar cells, b) *J–V* curves of the champion device and related parameters, c) energy level diagram of semiconductors and electrodes used in this study.

properties in these three regions to correlate device performance and charge carrier properties. Moreover, in-depth morphology characterization utilizing atomic force microscopy (AFM) and 2D grazing incidence wide angle X-ray scattering (GIWAXS) further explored the microstructure evolution as a function of blend ratio in both PBDB-T:ITIC and PBDB-T:N2200 blends. Finally, we looked at PCEs after thermal stressing; all-polymer devices exhibited significantly improved thermal stability relative to devices based on PBDB-T:ITIC. Our work discovered the high tolerance of all-polymer solar cells on its blend ratio. And we for the first time systematically studied the effect of blend ratio on morphology, efficiency and especially stability of all-polymer solar cells. The combinative results provide insights into future fabrication of large-area organic photovoltaics with long-term stability.

2. Results and Discussion

2.1. Materials and Solar Cell Performance

The inverted device structure of ITO/ZnO/active layer/MoO_x/Ag was adopted, and the chemical structures and energy levels of PBDB-T, N2200, and ITIC are shown in Figure 1. The energy levels of PBDB-T:ITIC and PBDB-T:N2200 can both form a type II band structure, allowing exciton dissociation at the donor/acceptor interface. The donor polymer material PBDB-T has a bandgap of 1.8 eV, the acceptor material ITIC has a low-lying lowest unoccupied molecular orbital (LUMO) energy level of −3.8 eV,[13] which provides an ≈0.3 eV offset for electron transfer from the LUMO of donor material to acceptor, and N2200 provides an ≈0.4 eV offset. The absorption of N2200 is broader than ITIC which is complementary to the absorption of PBDB-T. Throughout the experiments, PBDB-T:ITIC and PBDB-T:N2200 blends were cast from a fixed blend concentration of 20 and 8 mg mL^{-1}, respectively, according to their optimal processing condition. As shown in Figure 1b, the optimized PBDB-T:ITIC device had an open-circuit voltage (V_{oc}) of 0.88 V, a short-circuit current (J_{sc}) of 14.68 mA cm^{-2} and a fill factor (FF) of 70%, yielding a best PCE of 9.1%. The PBDB-T:N2200 device exhibited a V_{oc} of 0.85 V, a J_{sc} of 11.63 mA cm^{-2} and a FF of 64%, yielding a PCE of 6.33%, which was consistent with results obtained in previous work.[29,30] It is worth noting that the best device performance for PBDB-T:ITIC and PBDB-T:N2200 was achieved by adding 0.5% DIO into the processing solvent chlorobenzene.[30] According to previous reports, solar cells based on PBDB-T:ITIC and PBDB-T:N2200 processed from pure chlorobenzene without the additive DIO exhibited comparable PCEs relative to the best ones.[30] We then investigated the impact of D:A blend ratio and thermal treatment on device performance using device's cast from pure solvent chlorobenzene.

2.2. The Impact of D:A Blend Ratio on Solar Cell Performance

In order to investigate the effect of D:A weight ratio on device performance, we fabricated and compared the performance of nonfullerene OSCs based on PBDB-T:acceptor at varying weight blend ratios, from 1:10 to 20:1. The normalized device parameters including J_{sc}, V_{oc}, FF, and PCE under AM 1.5G, 100 mW cm^{-2} illumination were measured (**Figure 2**), the corresponding data are listed in Tables S1 and S2 (Supporting Information). The V_{oc} decreases at low and high acceptor ratios in PBDB-T:ITIC based devices, ranging from 0.81 to 0.90 V. In contrast, the V_{oc} of PBDB-T:N2200-based devices were relatively stable around 0.84 V across the entire D:A ratio range from 1:10 to 20:1. To study the evolution of other photovoltaic parameters, we defined three regions based on the D:A ratio: Region I: D:A blend weight ratio < 1:3; Region II: D:A blend weight ratio from 1:3 to 3:1 (contains maximum PCE); and Region III: D:A blend weight ratio > 3:1. Examining PBDB-T:ITIC devices in Region I, as the donor PBDB-T content increases, the FF steadily increases, while the J_{sc} drastically increases from 4.94 to 11.35 mA cm^{-2}, likely due to the enhanced absorption from the donor polymer. As a result, the device PCE is also improved with more PBDB-T. For PBDB-T:N2200 devices in Region I, when D:A ratio increases from 1:10 to 1:3, both the J_{sc} and PCE are enhanced significantly, while the FF keeps almost the same which suggests that the donor polymer can maintain high mobility at very low content in ITIC matrix. In Region II, maximum J_{sc} and PCE are obtained for both PBDB-T:ITIC and

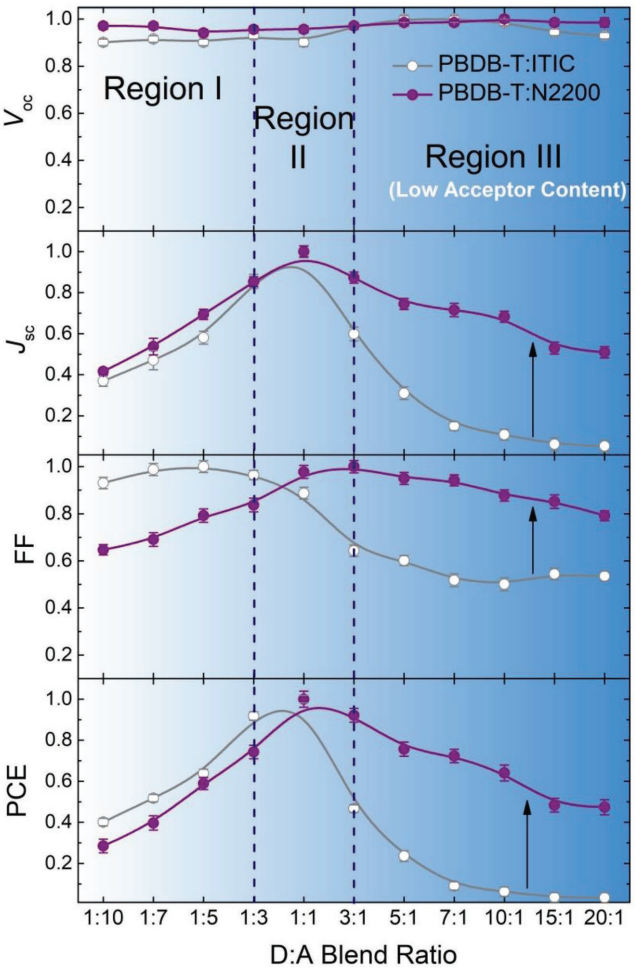

Figure 2. Summary plots of PBDB-T:ITIC (gray) and PBDB-T:N2200 (purple) solar cells performance at different D:A blend ratios.

PBDB-T:N2200 based devices. However, the influence of D:A ratio on FF is different for the two blends. We speculate that the difference is largely caused by the balance of electron and hole transport with the increase of donor content. In Region III: Except V_{oc}, all the photovoltaic parameters drop rapidly for PBDB-T:ITIC-based devices as the acceptor content is further reduced. At the D:A blend ratio of 10:1, the PCE dramatically decreases to less than 1.0%, indicating that the polymer/molecule device is quite sensitive on the acceptor loading. However, solar cell devices based on PBDB-T:N2200 show well-maintained PCE values in a wide range of blend ratios. For example, the PCE of all-polymer solar cells still maintain 64% and 47% of the optimal value at an extremely low D:A ratio of 10:1 and 20:1 respectively, showing high tolerance on acceptor content. To further investigate this feature of all-polymer solar cells, we also fabricated devices based on P2F-DO:N2200[35] with different D:A blend ratios. As shown in Figure S1 (Supporting Information), the PCE can still maintain 66% of the optimal value at an extremely low D:A ratio of 10:1, these results certainly demonstrated this may be unique properties for all-polymer solar cells.

We also investigated the photodiode behavior and the dark *J*–*V* characteristics of these devices were measured. As shown in **Figure 3**a,b, all-polymer devices exhibited relatively low leakage current under reverse bias at a wide range of blend ratios. They show good diode characteristics even at extremely low acceptor ratio (20:1). The slightly lower forward current at low donor content is likely due to the limited hole transport. In contrast, the dark *J*–*V* characteristics of PBDB-T:ITIC blends exhibit a evidently different trend. The devices show very poor diode properties at D:A ratio of 10:1 and 20:1, which is consistent with the decreased photovoltaic parameters at low acceptor content, suggesting imbalanced carrier transport and more charge recombination in the device. Incident photon-to-current efficiency (IPCE) of both PBDB-T:ITIC and PBDB-T:N2200-based devices with different D:A blend ratios were investigated to confirm these results. All the J_{sc} values from the *J*–*V* measurements matched well with the integrated J_{sc} values obtained from the IPCE spectra (Figure 3c,d). We notice that the contribution of ITIC (≈700–800 nm) to the photocurrent at the optimal D:A ratio is significantly higher than that of N2200, partially due to the higher absorption of ITIC (see Figures S2 S3 in the Supporting Information). At D:A ratio of 10:1 and 20:1, both polymer and molecule acceptor show little contribution to the IPCE because of their negligible absorption at this low loading. However, it is worth noting that the IPCE contribution from PBDB-T (between 300 and 700 nm[36]) can still maintain a relatively high value when blending with N2200, while it is largely reduced with ITIC as the acceptor. The result indicates that N2200 can better keep good electron transport at very low loading than ITIC.

2.3. Charge Generation, Transfer, and Transport Properties of Different D:A Blend Ratios

In order to further understand the charge generation and extraction process in PBDB-T:ITIC and PBDB-T:N2200 solar cells influenced by different D:A ratios, we measured the change of photocurrent density (J_{ph}) as a function of effect voltage (V_{eff}) under illumination at 100 mW cm^{-2}.[37] As shown in **Figure 4**a, at low V_{eff} below 0.6 V, the J_{ph} of PBDB-T:N2200

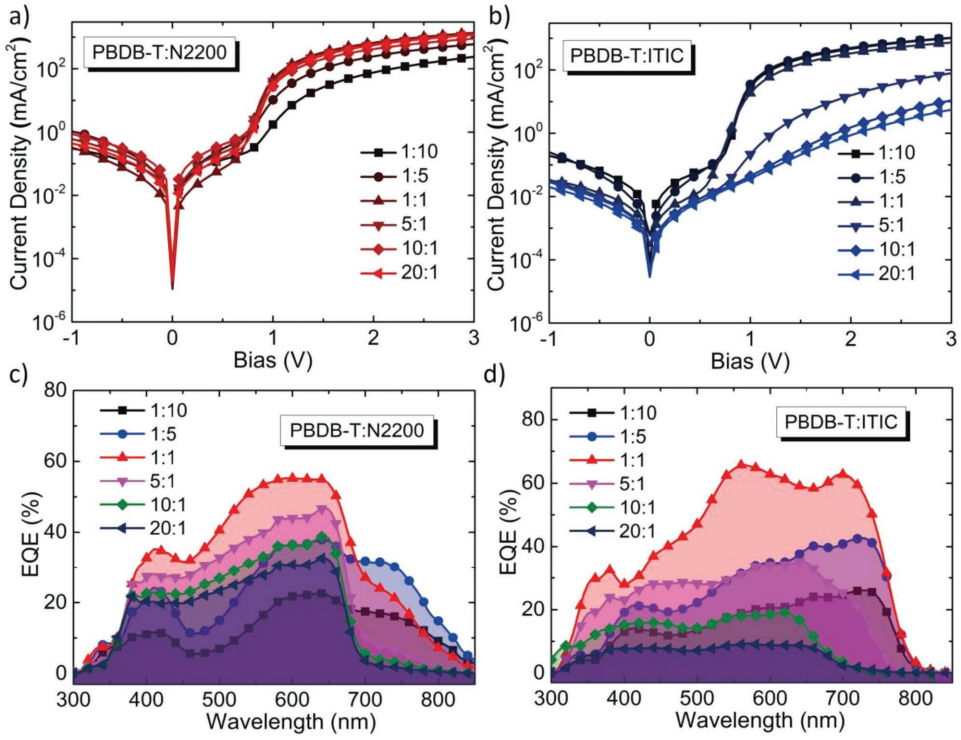

Figure 3. a) Dark *J*–*V* curves of PBDB-T:N2200 with different D:A blend ratios, b) dark *J*–*V* curves of PBDB-T:ITIC at different D:A blend ratios, c) EQE curves of PBDB-T:N2200 devices at different D:A blend ratios, d) EQE curves of PBDB-T:ITIC devices at different D:A blend ratios.

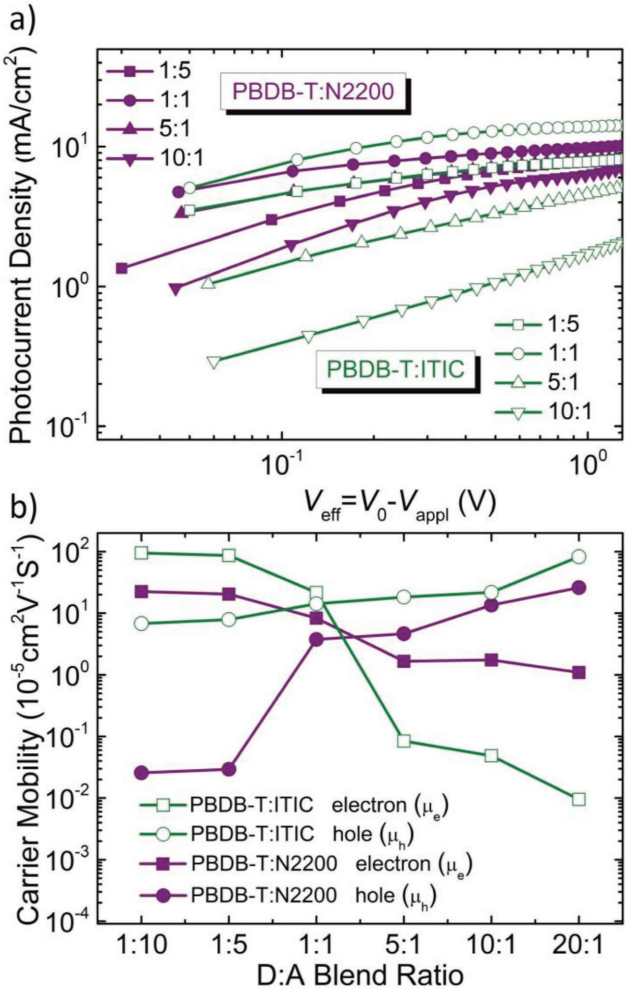

Figure 4. a) Photocurrent of PBDB-T:ITIC (green) and PBDB-T:N2200 (purple) with different D:A blend ratios. b) Electron mobilities (μ_e) and hole mobilities (μ_h) of PBDB-T:ITIC (green) and PBDB-T:N2200 (purple) at different D:A blend ratios.

devices increase and reach saturation with similar trend, indicating efficient carriers collection for different blend ratios. In contrast, for PBDB-T:ITIC with low acceptor content, the J_{ph} increases nearly linearly without saturation at high values of V_{eff}, indicating V_{eff}-dependent carrier transport in these low-acceptor-content devices due to small electron mobility. Meanwhile, the saturation current for PBDB-T:N2200 is similar for all blend ratios, suggesting weak dependence of charge generation on acceptor content. For PBDB-T:ITIC devices, the values are very sensitive to the blend ratios, which implies that the blend ratios may significantly affect the film morphology and hence charge generation. We hypothesize that small amount of molecular acceptor ITIC will form isolated domains, leading to reduced D:A interface and carrier transport paths, while polymer acceptor N2200 with long chain can still develop percolation network at low content. Photoluminescence (PL) studies were then carried out to compare the PL quenching efficiency as shown in Figure S4 (Supporting Information). The decrease of PL peak indicates that generated excitons are efficiently quenched.[38] The PL peak intensities of the blend films relative to those of the neat films at similar thicknesses reflect the efficiency of exciton diffusion and dissociation at the D:A interface, granting insight into the nanoscale morphology.[39] The PL quenching of the acceptor emission peak was more efficient in PBDB-T:ITIC system, suggesting efficient hole transfer from acceptor ITIC excitons to the PBDB-T donor polymer, which has been reported in previous work.[40] In addition, the PL quenching of the PBDB-T donor emission peak was more efficient in PBDB-T:ITIC system at the optimal content. However, at the D:A ratio of 10:1, the PL quenching efficiency of both PBDB-T and ITIC is worse than that in PBDB-T:N2200 blend, resulting in less efficient charge generation, which is consistent with our aforementioned hypothesis.

Besides charge generation, charge transport is also crucial for efficient OSCs. Both electron and hole mobility are important to achieve efficient and balanced carrier transport.[41] Carrier mobility of both donor and acceptor materials will be affected by the blend ratios and morphology of the blend film. The bulk charge transport properties of PBDB-T:ITIC and PBDB-T:N2200 blend films were investigated by using the space-charge-limited-current method.[42] The hole mobilities were measured with a device structure of ITO/ PEDOT:PSS/ active layer/MoO_x/Ag, and the electron mobilities were measured with a device structure of ITO/ZnO/active layer/LiF/Ag (Figure 4b; see Figures S5 and S6 for *J–V* characteristics and Table S3 for parameters in the Supporting Information). When tuning the D:A blend ratios from 1:10 to 20:1, the hole mobility of the PBDB-T:ITIC blend rises gently with increased donor loading, while the hole mobility of the PBDB-T:N2200 blend rises drastically at first and then slowly increases after reaching the optimal D:A ratio. For the electron mobility in PBDB-T:ITIC blend film, it drops rapidly at low ITIC loading, while the reduction trend is much slower for PBDB-T:N2200 blend. The electron and hole mobilities are balanced when the D:A ratio is 1:1 and 2:1 for PBDB-T:ITIC and PBDB-T:N2200, respectively, which is consistent with their optimized device performance. When the D:A blend ratio is higher than 2:1, the value of μ_h/μ_e in PBDB-T:ITIC-based devices increases faster than that in PBDB-T:N2200-based devices. The balance of carrier transport is in strong correlation with the device FF, which may be one of the main reasons for the relatively low performance of PBDB-T:ITIC devices with low acceptor content. All these results demonstrate that charge carrier mobilities in PBDB-T:N2200 blend films are more balanced and more resilient to changes in blend ratios compared to PBDB-T:ITIC blends.

2.4. The Impact of D:A Blend Ratio on Nonfullerene Blend Morphology

The effect of blend ratios on device charge generation and transport is very likely linked to the film morphology. It is well-known that a bi-continuous interpenetrating network in polymer solar cells is necessary for the transport of holes and electrons.[43,44] To better understand the relationship between active layer morphology and D:A ratios, the microstructures of both PBDB-T:ITIC and PBDB-T:N2200 blends were investigated using AFM and 2D GIWAXS.[45–47] AFM images show the surface topography of BHJ blend films with different composition.

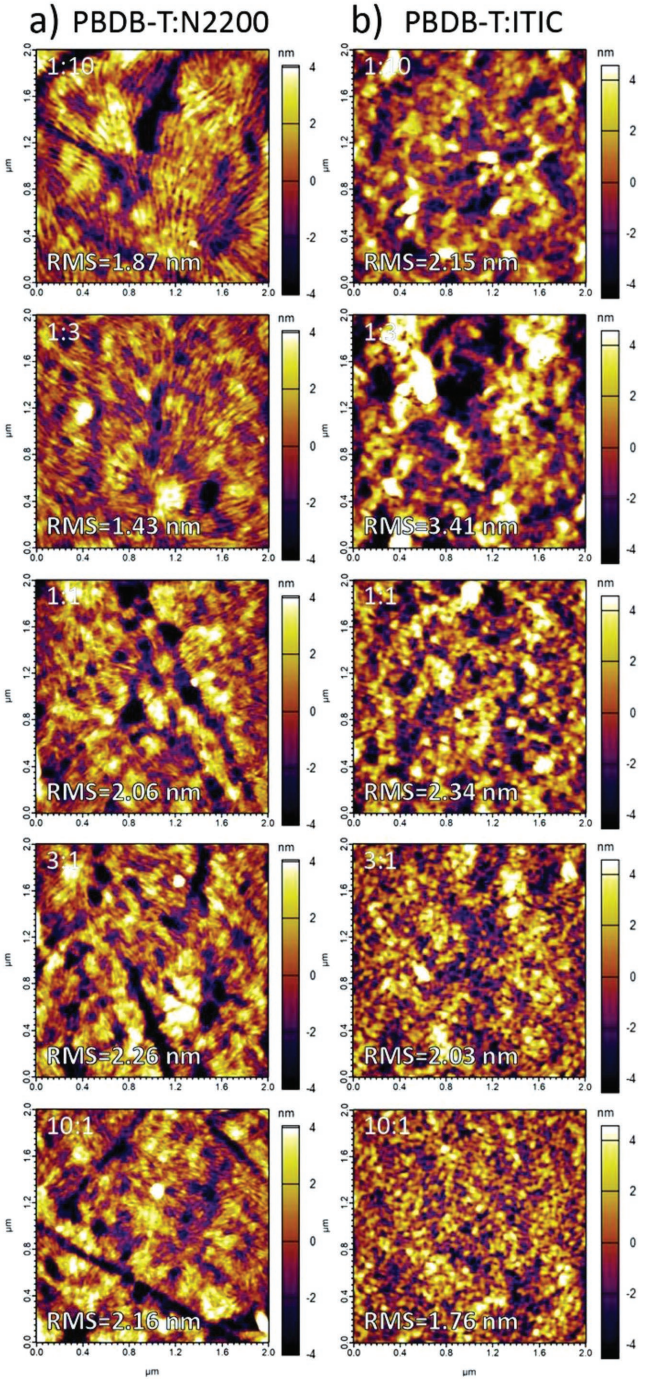

Figure 5. a) AFM height images for PBDB-T:N2200 at D:A blend ratio of 1:10, 1:3, 1:1, 3:1, 10:1, b) PBDB-T:ITIC at D:A blend ratios of 1:10, 1:3, 1:1, 3:1, 10:1.

As shown in **Figure 5** and Figure S7 (Supporting Information), all blend films are relatively uniform with smooth surface morphology. The evolution of the surface morphology as a function of D:A blend ratio for PBDB-T:N2200 is shown in Figure 5a. The PBDB-T:N2200 blend film with D:A ratio of 1:10 forms relatively large fibril aggregation with ordered structures, since N2200 is generally found to be a highly crystalline polymer.[48–50] With the decrease of N2200 ratio in the blend, the ordered structure is less distinct but still visible, indicating well maintained N2200 network inside the PBDB-T matrix even at extremely low acceptor content. In contrast, in PBDB-T:ITIC blends we can only observe large aggregations likely formed by small molecule ITIC which will be less apparent with lower ITIC content, as shown in Figure 5b. At the D:A ratio of 20:1, the film looks totally covered by amorphous PBDB-T. We do not observe long-range ordered structure from ITIC, suggesting less well-developed network structure and hence poor electron transport. Since AFM only probes the film surface morphology, in order to gain insight into the crystallinity and structural order inside these nonfullerene blends at different D:A weight ratios, we studied the morphology of both PBDB-T:ITIC and PBDB-T:N2200 using 2D GIWAXS. Figure S8 (Supporting Information) shows the scattering images of pristine PBDB-T, ITIC, and N2200. Neat N2200 film exhibits a broad and relatively strong scattering peak due to π–π stacking in the out-of-plane direction at ≈1.6 Å, which corresponded to a preferable face-on orientation in the film. In addition, neat N2200 film exhibits multiple diffraction peaks in the in-plane direction, attributed to alkyl stacking, suggesting well-ordered structure in the film. In contrast, the packing and orientation of PBDB-T and ITIC films are less anisotropic. For the neat materials, the corresponding "π–π stacking" distance is 3.98, 4.30, and 4.11 Å for PBDB-T, ITIC, and N2200, respectively.

GIWAXS of both PBDB-T:ITIC and PBDB-T:N2200 blend films with different D:A weight ratios were also measured (**Figure 6**). The 2D GIWAXS patterns of PBDB-T:N2200 exhibit similar trends in comparison with those of PBDB-T:ITIC blends. With low donor (1:10) or acceptor (10:1) content, the diffraction peaks are dominated by the main materials. At more balanced D:A blend ratios (1:3, 1:1, and 3:1), the (010) peak of the acceptor for both blend film is less prominent, likely due to the reduction of acceptor domains and the intercalation of PBDB-T phase. However, both D/A phases can still show their diffraction peak, indicating appropriate aggregation and fine phase separation, consistent with the optimal charge transport and photovoltaic performance at these ratios. Note that the evolution of scattering patterns as a function of D:A blend ratios is similar for both blend films in Region I, II, and III. However, solar cell performance of PBDB-T:ITIC and PBDB-T:N2200 shows similar change only in Region I (D:A ratio: 1:10 to 1:3) and Region II (D:A ratio: 1:3 to 3:1), with distinct difference in Region III. One possible explanation is that the interconnectivity of conjugated molecules like ITIC is largely reduced at low content relative to conjugated polymers, thus limiting carrier transport. To verify that, we can see the line-cuts of the spectra shown in Figure 6c. Since the scattering peaks of the acceptor are hard to observe at low acceptor content, we can focus on the patterns of the donor PBDB-T. We can clearly observe that the donor scattering peak at 0.3 $Å^{-1}$ is getting more pronounced at the D:A ratio of 10:1 for ITIC system, indicating the forming of large and high-purity PBDB-T domains. Considering the very small amount of ITIC, we can expect poor interconnection between acceptor domains. Thus at the D:A ratio of 10:1, the charge generation and transport are not efficient. In contrast, the donor scattering peak at 0.3 $Å^{-1}$ is less pronounced for PBDB-T:N2200 system at low acceptor content,

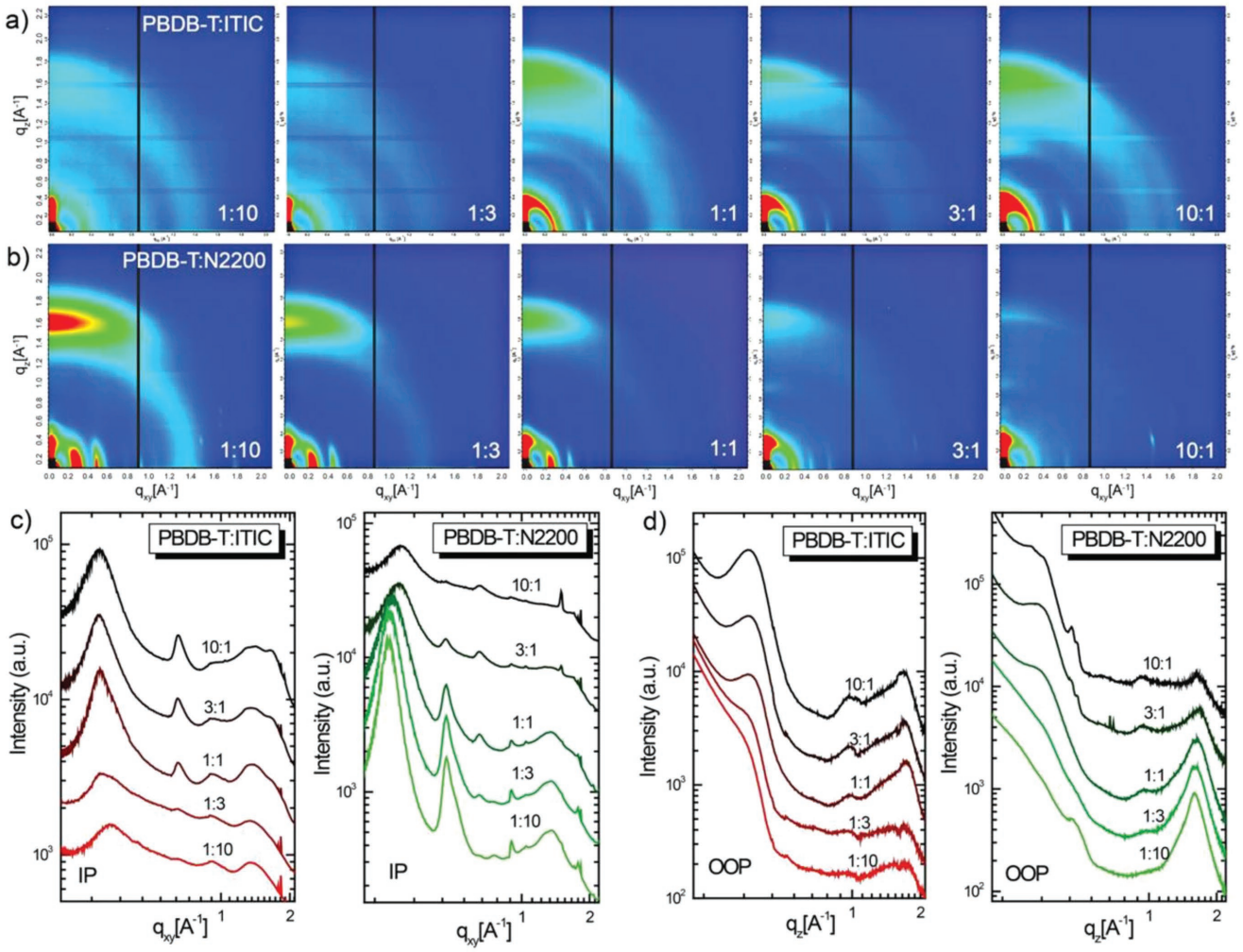

Figure 6. a) 2D GIWAX patterns of PBDB-T:ITIC film at D:A blend ratio of 1:10, 1:3, 1:1, 3:1, 10:1, b) 2D GIWAX patterns of PBDB-T:N2200 at D:A blend ratio of 1:10, 1:3, 1:1, 3:1, 10:1, c) sector plots in the in-plane and out-of-plane direction of each film. Faint lines in some of the images are artifacts due to changes in baseline during the timescale of the analysis; they will not interfere with peak analysis.

which suggests that a fair amount of N2200 still exist in the PBDB-T domains, resulting in fine phase separation and interconnected domains. As a result, the polymer:polymer system shows significantly better performance at low acceptor content than polymer:molecule system. To make it clear, we propose a schematic illustration for the nonfullerene BHJ blend morphology of the two compared systems, as shown in **Figure 7**. In relatively high acceptor region (Region I, Figure 7a,d), the performance is limited by the aggregation and connectivity of PBDB-T, and so both blends exhibit comparable performance. At a more balanced D:A ratio region (Region II, Figure 7b,e), the heterojunctions between donor polymer and acceptor phase are optimized and result in efficient charge separation and balanced transport. The optimal PCE of PBDB-T:N2200 is lower compared to that of optimal PBDB-T:ITIC device, which may be attributed to the relatively less efficient charge generation and separation of N2200 than ITIC.[44] At the extremely low acceptor region (Region III, Figure 7c,f), for PBDB-T:ITIC, ITIC domains may have less interconnectivity, resulting in inefficient separation of geminate pairs and increased bimolecular recombination of free carriers. In contrast, PBDB-T:N2200 blends exhibit less decreased performance as N2200 is reduced, likely due to the well maintained electron transport-path. This model is in good agreement with the morphology characterization as well as photovoltaic performance of the all-polymer and polymer–molecule devices.

2.5. The Stability of Nonfullerene Solar Cells

The stability of solar cell under thermal stress is an essential consideration for the practical application.[51–53] One of the main obstacles for fullerene-based acceptors like PCBM is that aggregates and crystallites appear in the blend upon heating and lighting.[54,55] In this regard, the relative morphological stability of organic nonfullerene blends is worthy of studying. We first investigated the stability of PBDB-T:ITIC, PBDB-T:N2200 without DIO under dark conditions in an N_2 glovebox without encapsulation. Aging measurements were also carried out for devices of PBDB-T:N2200 with a low acceptor content at D:A

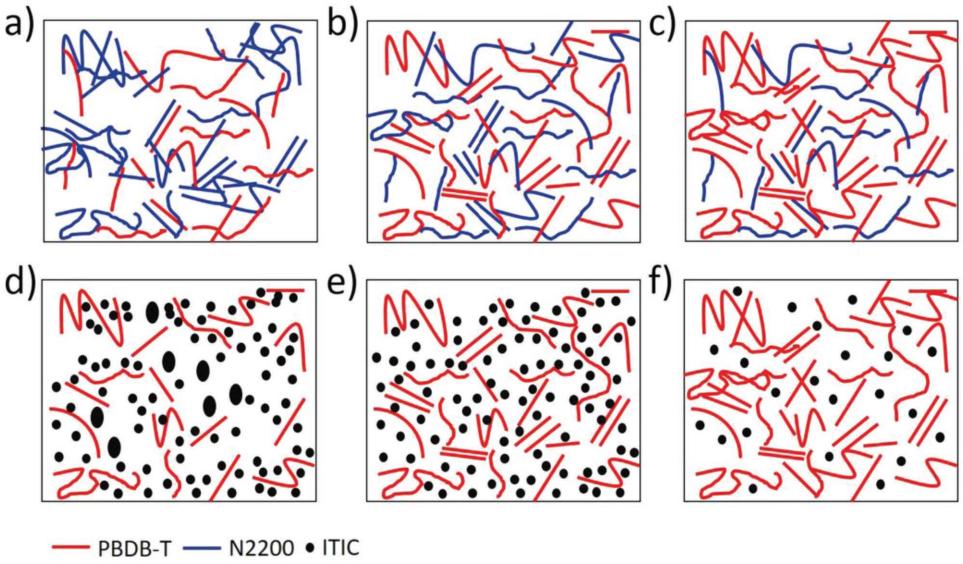

Figure 7. a) Cartoon illustration of the morphology of blend film of PBDB-T:N2200 with high acceptor concentration, b) optimal D:A blend ratio, and c) low acceptor concentration, d) cartoon illustration of the morphology of blend film of PBDB-T:ITIC with high acceptor concentration, e) optimal D:A blend ratio, and f) low acceptor concentration.

ratio of 10:1 to study the possible effect of ratio on device stability. Meanwhile, since the PBDB-T:ITIC device with low acceptor content had an extremely low efficiency, its stability was not investigated. All blends were processed and treated identically. After the initial measurement, devices were stored under dark condition in a glovebox without encapsulation, and the measurements were performed at regular intervals over the course of ≈70 d. As shown in **Figure 8**a, Figures S9 and S10 (Supporting Information), PBDB-T:N2200 with D:A ratio of 10:1 demonstrates the least degradation. After an initial small drop in performance within the first 30 h, the PCE improves slowly and gives the best performance after 1700 h. The PCE of PBDB-T:N2200 solar cell with D:A ratio of 1:1 remains relatively stable and gives 88% of the initial after 1700 h aging. PBDB-T:ITIC cell with D:A ratio of 1:1 remains a similar value of 89% of the initial performance during the same aging period. In short, without annealing all the three devices show stable performance for at least 70 d under N_2.

Finally, we investigated the stability of nonfullerene solar cell devices under thermal stress. After the initial measurement was taken, devices were stored on a hot plate at 80 °C in a glovebox without encapsulation between measurements. The measurements were taken at regular intervals over the course of 70 d. From Figure 8b, both PBDB-T:N2200-based devices exhibit excellent stability under continuous heating with very slight PCE degradation after 1700 h thermal treatment. In contrast, the efficiency of PBDB-T:ITIC nonfullerene solar cells deteriorates quickly and falls to 76% of the initial value within the first 8 h. In the end of the stability study,

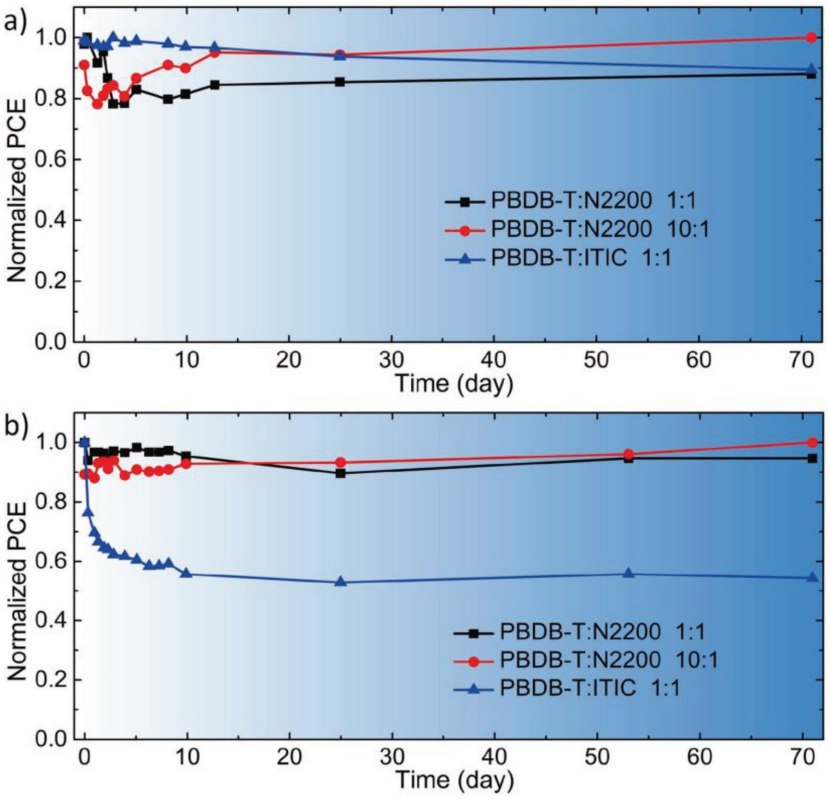

Figure 8. a) Stability of solar cell devices based on PBDB-T:N2200 (D:A = 1:1 and 10:1) PBDB-T:ITIC (D:A = 1:1) under the dark condition, b) thermal stability of solar cell devices based on PBDB-T:N2200 (D:A = 1:1 and 10:1) PBDB-T:ITIC (D:A = 1:1).

the PCE further drops to 54% of the initial value. The stable PCE values of all-polymer solar cells compared to polymer–molecule cells are encouraging. We speculate that all-polymer blend can better retain their morphology under thermal stress than polymer–molecule blend, since the morphology of system based on small molecule is more sensitive to heating as previously reported. In addition, it seems that the large reduction of acceptor polymer content will not decrease the stability of all-polymer solar cells. Thus excellent device stability for all-polymer solar cells can be realized despite the variation of blend ratios. In short, our work reveals the potential of all-polymer solar cells for designing of stable, scalable solar cells with practical operating lifetimes.

3. Conclusion

In summary, we comparatively investigated the impact of D:A blend ratio on the device performance of two representative BHJ nonfullerene organic solar cells using PBDB-T as the donor and widely used small molecule ITIC or polymer N2200 as the acceptors. In addition, we also measured the thermal stability of ITIC and N2200-based solar cells. We found that the PCE of all- polymer solar cells shows apparently higher tolerance to blend-ratio changes, compared with polymer–molecule-based devices. In addition, all-polymer solar cells, despite D:A blend ratio, are stable (less than 5% PCE loss) at least over 70 d under continuous heating at 80 °C in a glovebox without encapsulation. In contrast, the efficiency of PBDB-T:ITIC-based nonfullerene solar cells deteriorates quickly and falls to 54% of the initial value. A detailed morphology characterization along with charge carrier transport investigation reveals that the morphology-affected electron transport plays an import role. Our work demonstrated that all-polymer solar cells show advantage in operational lifetime under thermal stress and blend-ratio resilience, which indicates their high potential for designing of stable and scalable solar cells.

4. Experimental Section

Materials and Characterization: PBDB-T was synthesized according to the previous report by Hou and co-workers, and N2200 was synthesized following the methods in the previous works.[31,34] ITIC was obtained from Solarmer Materials Inc. Unless otherwise stated, all chemicals were commercially available products and used as received. UV–vis-NIR spectra were recorded on a Perkin Elmer model Lambda 750. AFM images were measured with an Asylum Research Cypher S AFM microscope. 2D GIWAXS measurements were performed at the Advanced Light Source (ALS)-Lawrence Berkeley National Laboratory on Beamline 7.3.3.

Solar Cells Device Fabrication and Characterization: Organic solar cells were fabricated with a structure of ITO/ZnO/active layer/MoO_x/Ag. ITO-coated glass substrates were cleaned sequentially with acetone, deionized water, isopropanol, and acetone for 20 min each time, and then treated with UV–ozone for 30 min. ZnO thin films spin-coated onto ITO substrates were obtained from ZnO precursor solution by sol–gel method at 4000 rpm and then annealing for 10 min at 200 °C in air. Before spin coating of the active layer, the solution should be kept heating at 40 °C for at least 6 h. The solvent was chlorobenzene with a concentration of 20 mg mL^{-1} for PBDB-T:ITIC and 8 mg mL^{-1} for PBDB-T:N2200. Blend solution of donor and acceptor with weight ratio of 1:10, 1:7, 1:5, 1:3, 1:1, 3:1, 5:1, 7:1, 10:1, 15:1, and 20:1 were spin coated onto the ZnO layer at 2500 rpm. After spin coating, the active layer of PBDB-T:ITIC was annealed for 10 min at 120 °C in N_2-atmosphere glovebox. For device preparation, silver (Ag) (100 nm) as the cathode was deposited on the MoO_x (10 nm) in vacuum thermal evaporator. The area of each device is 7.25 mm^2. The performance of all cells was tested under AM 1.5G light (Newport, Class AAA solar simulator, 94023A-U). The external quantum efficiency (EQE) was determined using certified IPCE equipment (Zolix Instruments, Inc, SolarCellScan100).

Supporting Information

Supporting Information is available from the Wiley Online Library or from the author.

Acknowledgements

This work was supported by the National Key Research Projects (Grant No. 2016YFA0202402), the Natural Science Foundation of Jiangsu Province of China (BK20170337), the National Natural Science Foundation of China (Grant Nos. 51761145013 and 61674111), and "111" projects. The authors thank the Collaborative Innovation Center of Suzhou Nano Science and Technology, Soochow University. The authors also acknowledge the great help from Prof. Guillermo C. Bazan at University of California, Santa Barbara, and Priority Academic Program Development of Jiangsu Higher Education Institutions (PAPD). GIWAXS measurements were taken at Advanced Light Source (ALS)-Lawrence Berkeley National Laboratory on Beamline 7.3.3.

Conflict of Interest

The authors declare no conflict of interest.

Keywords

D:A blend ratio, electron acceptors, nonfullerene polymer solar cells, stability

Received: January 4, 2018
Revised: January 22, 2018
Published online: March 12, 2018

[1] G. Yu, J. Gao, J. C. Hummelen, F. Wudl, A. J. Heeger, *Science* **1995**, *270*, 1789.
[2] A. Mishra, P. Bäuerle, *Angew. Chem., Int. Ed.* **2012**, *51*, 2020.
[3] Y. Lin, Y. Li, X. Zhan, *Chem. Soc. Rev.* **2012**, *41*, 4245.
[4] X. Zhan, Z. A. Tan, B. Domercq, Z. An, X. Zhang, S. Barlow, Y. Li, D. Zhu, B. Kippelen, S. R. Marder, *J. Am. Chem. Soc.* **2007**, *129*, 7246.
[5] N. C. Cates, R. Gysel, Z. Beiley, C. E. Miller, M. F. Toney, M. Heeney, I. McCulloch, M. D. McGehee, *Nano Lett.* **2009**, *9*, 4153.
[6] A. Facchetti, *Mater. Today* **2013**, *16*, 123.
[7] P. A. Troshin, H. Hoppe, J. Renz, M. Egginger, J. Y. Mayorova, A. E. Goryachev, A. S. Peregudov, R. N. Lyubovskaya, G. Gobsch, N. S. Sariciftci, V. F. Razumov, *Adv. Funct. Mater.* **2009**, *19*, 779.
[8] J. Yuan, C. McDowell, C.-K. Mai, G. C. Bazan, W. Ma, *Chem. Mater.* **2016**, *28*, 7479.
[9] J. Yuan, H. Dong, M. Li, X. Huang, J. Zhong, Y. Li, W. Ma, *Adv. Mater.* **2014**, *26*, 3624.

[10] D. Qian, W. Ma, Z. Li, X. Guo, S. Zhang, L. Ye, H. Ade, Z. Tan, J. Hou, *J. Am. Chem. Soc.* **2013**, *135*, 8464.
[11] T. Kim, J.-H. Kim, T. E. Kang, C. Lee, H. Kang, M. Shin, C. Wang, B. Ma, U. Jeong, T.-S. Kim, B. J. Kim, *Nat. Commun.* **2015**, *6*, 8547.
[12] S. H. Park, A. Roy, S. Beaupre, S. Cho, N. Coates, J. S. Moon, D. Moses, M. Leclerc, K. Lee, A. J. Heeger, *Nat. Photonics* **2009**, *3*, 297.
[13] Y. Lin, J. Wang, Z. G. Zhang, H. Bai, Y. Li, D. Zhu, X. Zhan, *Adv. Mater.* **2015**, *27*, 1170.
[14] B. Fan, L. Ying, P. Zhu, F. Pan, F. Liu, J. Chen, F. Huang, Y. Cao, *Adv. Mater.* **2017**, *29*, 1703906.
[15] W. Zhao, S. Li, H. Yao, S. Zhang, Y. Zhang, B. Yang, J. Hou, *J. Am. Chem. Soc.* **2017**, *139*, 7148.
[16] K. Zhang, Y. Qin, F. Li, L. Yu, M. Sun, *J. Phys. Chem. C.* **2017**, *121*, 19634.
[17] Z. Liu, D. Liu, K. Zhang, T. Zhu, Y. Zhong, F. Li, Y. Li, M. Sun, R. Yang, *J. Mater. Chem. A* **2017**, *5*, 21650.
[18] J. Zhu, S. Li, X. Liu, H. Yao, F. Wang, S. Zhang, M. Sun, J. Hou, *J. Mater. Chem. A* **2017**, *5*, 15175.
[19] J. Yuan, M. J. Ford, Y. Xu, Y. Zhang, G. C. Bazan, W. Ma, *Adv. Energy Mater.* **2018**, https://doi.org/10.1002/aenm.201703291.
[20] B. C. Thompson, J. M. Frechet, *Angew. Chem., Int. Ed.* **2008**, *47*, 58.
[21] K. M. Coakley, M. D. McGehee, *Chem. Mater.* **2004**, *16*, 4533.
[22] C. R. McNeill, S. Westenhoff, C. Groves, R. H. Friend, N. C. Greenham, *J. Phys. Chem. C* **2007**, *111*, 19153.
[23] J. Yuan, M. J. Ford, Y. Zhang, H. Dong, Z. Li, Y. Li, T.-Q. Nguyen, G. C. Bazan, W. Ma, *Chem. Mater.* **2017**, *29*, 1758.
[24] J. K. Lee, W. L. Ma, C. J. Brabec, J. Yuen, J. S. Moon, J. Y. Kim, K. Lee, G. C. Bazan, A. J. Heeger, *J. Am. Chem. Soc.* **2008**, *130*, 3619.
[25] T. Kim, J. Choi, H. J. Kim, W. Lee, B. J. Kim, *Macromolecules* **2017**, *50*, 6861.
[26] X. Guo, M. Zhang, J. Tan, S. Zhang, L. Huo, W. Hu, Y. Li, J. Hou, *Adv. Mater.* **2012**, *24*, 6536.
[27] C. H. Y. Ho, S. H. Cheung, H.-W. Li, K. L. Chiu, Y. Cheng, H. Yin, M. H. Chan, F. So, S.-W. Tsang, S. K. So, *Adv. Energy Mater.* **2017**, *7*, 1602360.
[28] M. Zhang, H. Wang, H. Tian, Y. Geng, C. W. Tang, *Adv. Mater.* **2011**, *23*, 4960.
[29] W. Zhao, D. Qian, S. Zhang, S. Li, O. Inganas, F. Gao, J. Hou, *Adv. Mater.* **2016**, *28*, 4734.
[30] L. Ye, X. Jiao, M. Zhou, S. Zhang, H. Yao, W. Zhao, A. Xia, H. Ade, J. Hou, *Adv. Mater.* **2015**, *27*, 6046.
[31] Y. Xu, J. Yuan, J. Sun, Y. Zhang, X. Ling, H. Wu, G. Zhang, J. Chen, Y. Wang, W. Ma, *ACS Appl. Mater. Interfaces* **2018**, *10*, 2776.
[32] Y. Zhang, J. Yuan, J. Sun, G. Ding, L. Han, X. Ling, W. Ma, *ACS Appl. Mater. Interfaces* **2017**, *9*, 13396.
[33] S. Lee, J. Kong, K. Lee, *Adv. Energy Mater.* **2016**, *6*, 1600970.
[34] S. Kwon, H. Kang, J.-H. Lee, J. Lee, S. Hong, H. Kim, K. Lee, *Adv. Energy Mater.* **2017**, *7*, 1601496.
[35] J. Yuan, J. Gu, G. Shi, J. Sun, H.-Q. Wang, W. Ma, *Sci. Rep.* **2016**, *6*, 26459.
[36] D. Qian, L. Ye, M. Zhang, Y. Liang, L. Li, Y. Huang, X. Guo, S. Zhang, Z. A. Tan, J. Hou, *Macromolecules* **2012**, *45*, 9611.
[37] P. W. M. Blom, V. D. Mihailetchi, L. J. A. Koster, D. E. Markov, *Adv. Mater.* **2007**, *19*, 1551.
[38] Z. Li, X. Xu, W. Zhang, X. Meng, W. Ma, A. Yartsev, O. Inganas, M. R. Andersson, R. A. Janssen, E. Wang, *J. Am. Chem. Soc.* **2016**, *138*, 10935.
[39] J. Yuan, W. Ma, *J. Mater. Chem. A* **2015**, *3*, 7077.
[40] H. Bin, L. Gao, Z. G. Zhang, Y. Yang, Y. Zhang, C. Zhang, S. Chen, L. Xue, C. Yang, M. Xiao, Y. Li, *Nat. Commun.* **2016**, *7*, 13651.
[41] K. Walzer, B. Maennig, M. Pfeiffer, K. Leo, *Chem. Rev.* **2007**, *107*, 1233.
[42] P. N. Murgatroyd, *J. Phys. D: Appl. Phys.* **1970**, *3*, 151.
[43] H. Yan, B. A. Collins, E. Gann, C. Wang, H. Ade, C. R. McNeill, *ACS Nano* **2012**, *6*, 677.
[44] D. D. Nuzzo, A. Aguirre, M. Shahid, V. S. Gevaerts, S. C. Meskers, R. A. Janssen, *Adv. Mater.* **2010**, *22*, 4321.
[45] B. A. Collins, E. Gann, L. Guignard, X. He, C. R. McNeill, H. Ade, *J. Phys. Chem. Lett.* **2010**, *1*, 3160.
[46] B. A. Collins, J. R. Tumbleston, H. Ade, *J. Phys. Chem. Lett.* **2011**, *2*, 3135.
[47] B. A. Collins, Z. Li, J. R. Tumbleston, E. Gann, C. R. McNeill, H. Ade, *Adv. Energy Mater.* **2013**, *3*, 65.
[48] S. Shi, J. Yuan, G. Ding, M. Ford, K. Lu, G. Shi, J. Sun, X. Ling, Y. Li, W. Ma, *Adv. Funct. Mater.* **2016**, *26*, 5669.
[49] J. Yuan, W. Guo, Y. Xia, M. J. Ford, F. Jin, D. Liu, H. Zhao, O. Inganäs, G. C. Bazan, W. Ma, *Nano Energy* **2017**, *35*, 251.
[50] T. Liu, Y. Guo, Y. Yi, L. Huo, X. Xue, X. Sun, H. Fu, W. Xiong, D. Meng, Z. Wang, F. Liu, T. P. Russell, Y. Sun, *Adv. Mater.* **2016**, *28*, 10008.
[51] Z. Li, X. Xu, W. Zhang, Z. Genene, W. Mammo, A. Yartsev, M. R. Andersson, R. A. J. Janssen, E. Wang, *J. Mater. Chem. A* **2017**, *5*, 11693.
[52] S. Holliday, R. S. Ashraf, C. B. Nielsen, M. Kirkus, J. A. Rohr, C. H. Tan, E. Collado-Fregoso, A. C. Knall, J. R. Durrant, J. Nelson, I. McCulloch, *J. Am. Chem. Soc.* **2015**, *137*, 898.
[53] M. Jørgensen, K. Norrman, S. A. Gevorgyan, T. Tromholt, B. Andreasen, F. C. Krebs, *Adv. Mater.* **2012**, *24*, 580.
[54] S. Holliday, R. S. Ashraf, A. Wadsworth, D. Baran, S. A. Yousaf, C. B. Nielsen, C. H. Tan, S. D. Dimitrov, Z. Shang, N. Gasparini, M. Alamoudi, F. Laquai, C. J. Brabec, A. Salleo, J. R. Durrant, I. McCulloch, *Nat. Commun.* **2016**, *7*, 11585.
[55] Z. Li, W. Zhang, X. Xu, Z. Genene, D. D. Rasi, W. Mammo, A. Yartsev, M. R. Andersson, R. A. J. Janssen, E. Wang, *Adv. Energy Mater.* **2017**, *7*, 1602722.